3D Model for the Evaluation of Multiaxial Fracture Behavior of Reinforced Concrete Members

R. Cerioni, P. Bernardi, E. Michelini and A. Mordini

Department of Civil-Environmental Engineering and Architecture, University of Parma, Viale Usberti 181/A, 43124 Parma, Italy; Fax: +39 0521 905924; E-mail: roberto.cerioni@unipr.it

ABSTRACT. *A three-dimensional model for the analysis of RC members, with particular reference to the cracked stage, is proposed in terms of secant stiffness matrix. This formulation has been obtained by taking into account the flexibility contributions of cracks and of the concrete between adjacent cracks both in the singly and in the multi-cracked stages. The model includes all the interface phenomena generated along cracks, such as aggregate bridging and interlock, tension stiffening and dowel action. Finally, the model has been implemented into a Finite Element code and it has been validated through the comparison with significant experimental data.*

INTRODUCTION

The post-cracking behavior of reinforced concrete (RC) members is characterized by several complex aspects, such as the formation and reorientation of one or more cracks (Fig.1a), the interface actions at crack surfaces, the interaction effects between concrete and reinforcing bars, the non-linear compressive stress-strain relation for concrete and the markedly anisotropic behavior due to the arrangement of reinforcement (Fig. 1b).

In this study, a three-dimensional numerical model for the analysis of cracked RC elements subjected to a multiaxial state of stress is proposed. The model, named 3D-PARC [1], represents an extension of the previous 2D-PARC [2,3] and has been formulated in terms of secant stiffness matrix to allow the implementation into a FE procedure. In the uncracked stage, concrete behavior is described through a non-linear elastic model, the elastic moduli are evaluated through equivalent nonlinear uniaxial relationships and the maximum stresses are limited by an appropriate strength domain [1,4]. Singly and multi-cracked stages are simulated by adding crack contributions to the flexibility of the uncracked material, whose properties are properly degraded. These contributions are evaluated through a local analysis of the reinforced concrete element, on the basis of a strain decomposition procedure. The model assumes fixed, multi-directional cracking and smeared reinforcement approaches, taking into account the effects of a multiaxial stress state and several post-cracking phenomena, such as tension stiffening, dowel action and aggregate interlock. It has been implemented into a FE code and validated through the comparison with significant experimental data.

(a)

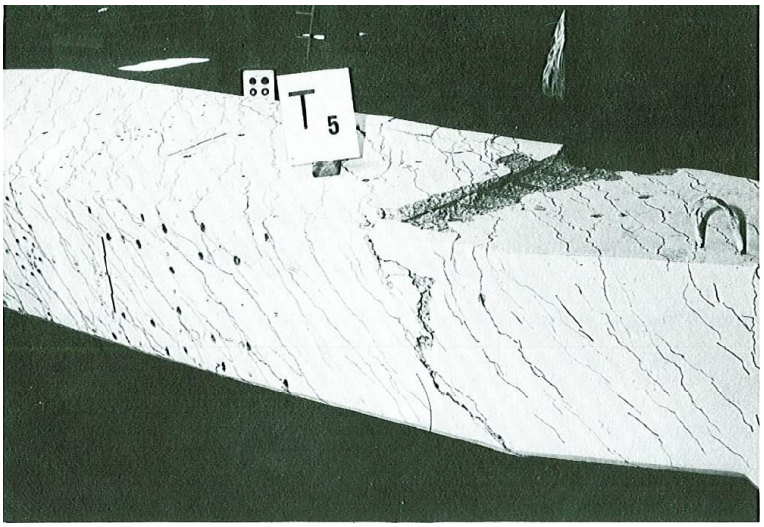

(b)

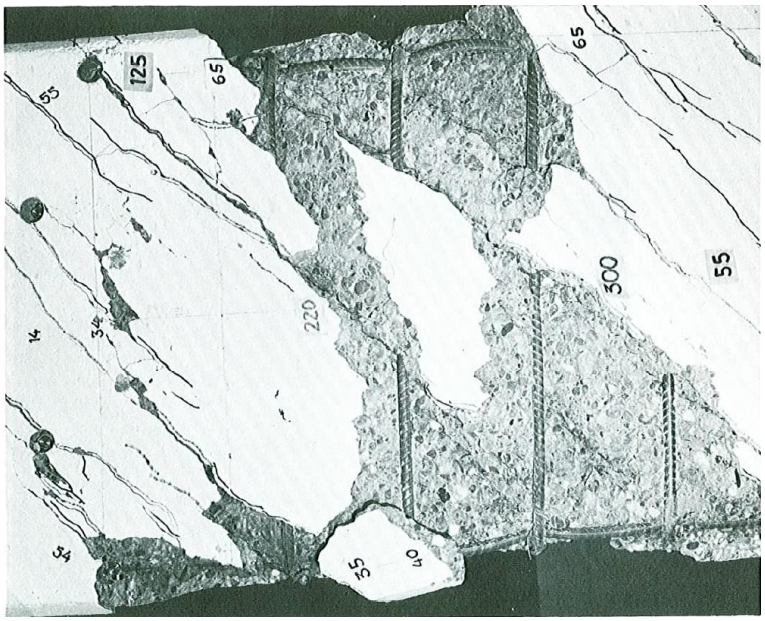

Figure 1. (a) Crack pattern in a RC beam subjected to torsion in correspondence of failure load; (b) typical reinforcement arrangement and crack orientation at failure [5].

CRACKED STAGE: INTERFACE PHENOMENA, STEEL BAR-CONCRETE INTERACTION, CONSTITUTIVE RELATIONSHIPS

The proposed model is structured in a modular framework. All the mechanical phenomena are individually analyzed on the basis of their properties and physical conditions, and the stiffness matrix is computed separately for each resistant contribution by using suitable constitutive models and techniques.

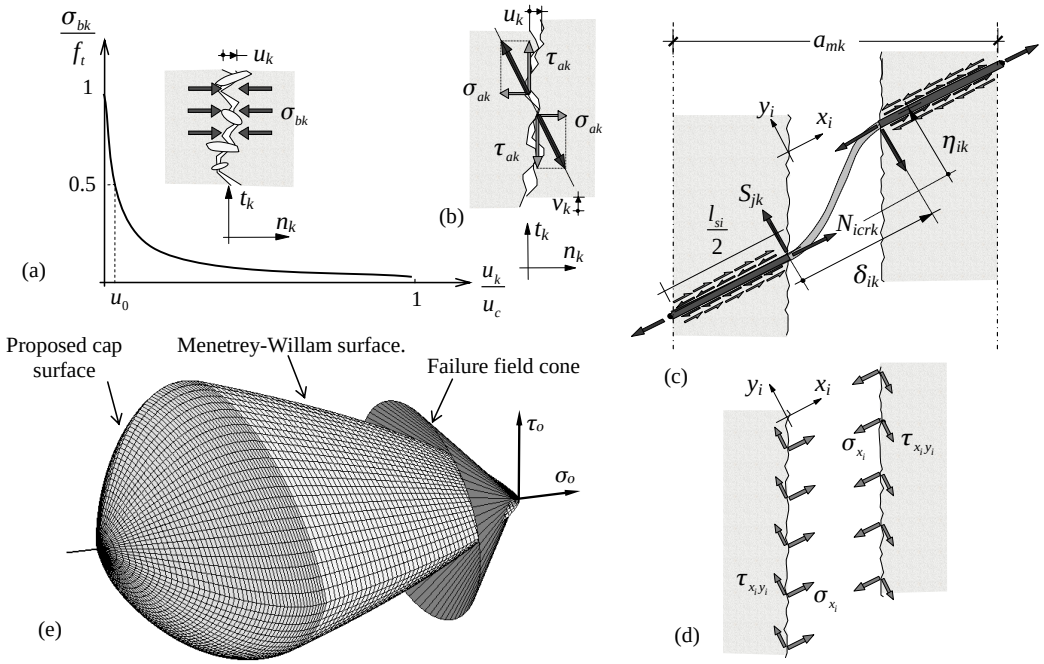

Figure 2. (a) Aggregate bridging and (b) interlock actions in the n_k - t_k plane; (c) steel contributions in the crack and (d) equivalent smeared stresses in the x_i-y_i plane; (e) failure surface and cone defining the failure modes.

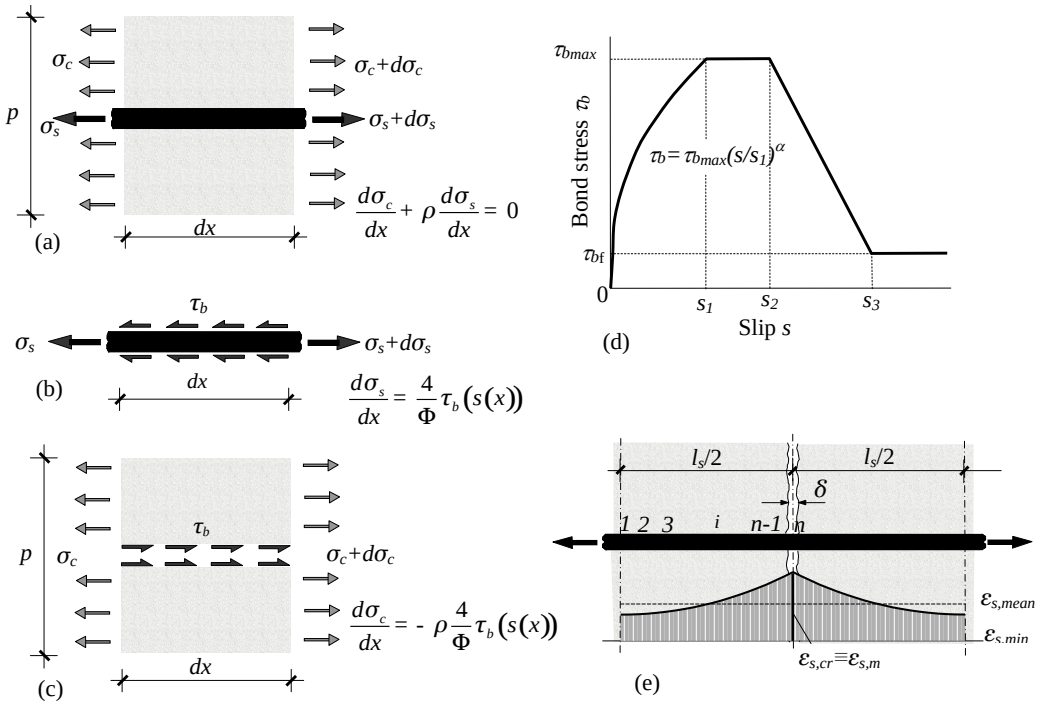

Figure 3. Equilibrium conditions of (a) RC element, (b) steel bar and (c) concrete; (d) CEB Model Code 90 bond-slip law; (e) finite difference discretization and final steel strain distribution.

Aggregate Bridging and Interlock Contributions

Aggregate bridging, which generates normal stresses transferred between crack surfaces (Fig.2a), is modeled by a smooth curve as a function of the k^{th} crack opening u_k [1,6]:

$$\sigma_{bk} = \frac{f_t}{1+(u_k/u_0)^p} = c_{bk}\frac{u_k}{a_{mk}} = c_{bk}\varepsilon_k \tag{1}$$

where c_{bk} is the bridging coefficient, u_0 is the crack opening corresponding to σ_{bk}=0.5 f_t, p is a coefficient which takes into account the properties of aggregates crossing the crack (in this work, p = 1 has been assumed) and a_{mk} is the crack spacing.

Aggregate interlock, which generates normal and shear stresses due to slip between crack surfaces (Fig.2b), is modeled by [7]:

$$\begin{aligned} \sigma_{ak} &= -c_{uvk}\gamma_k \\ \tau_{ak} &= c_{vk}\gamma_k \end{aligned} \tag{2}$$

The two coefficients are defined as functions of the crack opening and the crack slip:

$$c_{vk} = \tau^*\left(1-\sqrt{\frac{2u_k}{D_{\max}}}\right)\frac{a_3 + a_4|v_k/u_k|^3}{1+a_4(v_k/u_k)^4}\frac{a_{mk}}{u_k}\ ;\ c_{uvk} = \frac{a_1\cdot a_2}{u_k^{2q}}\left(1+\left(\frac{v_k}{u_k}\right)^2\right)^{-q} c_{vk}v_k \tag{3}$$

where: $\tau^* = 0.27\,f_c$, $q = 0.25$, $a_1a_2 = 0.62$, $a_3 = 2.45/\tau^*$, $a_4 = 2.44\left(1-4/\tau^*\right)$ and D_{max} is the maximum aggregate size.

Finally, the concrete stiffness matrix in the crack coordinate system n_k-t_k is obtained:

$$\left[D_{c,crk}^{n_k t_k}\right] = \begin{bmatrix} c_{bk} & -c_{uvk} \\ 0 & c_{vk} \end{bmatrix} \tag{4}$$

Dowel Action and Tension Stiffening Contributions

Steel bars which cross the k^{th} crack exhibit axial and transversal stiffness, the latter due to the dowel action contribution (Fig.2c). The axial and dowel actions are modeled in the local steel coordinate system x_i – y_i (Figs. 2c,4b) and then smeared on the crack surface, so obtaining equivalent stresses (Fig.2d). The axial and transversal displacements δ_{ik} and η_{ik}, along x_i and y_i , respectively, are evaluated as a function of the crack displacements u_k and v_k.

The dowel action contribution S_{ik}, modeled according to [8] and smeared, yields:

$$\tau_{ik} = 13.66\ f_c^{0.38}\phi_i^{-0.25}\rho_{\mathrm{si}}\frac{\mathrm{l}_{\mathrm{si}}}{(\delta_{ik}+0.2)\eta_{\mathrm{ik}}^{0.64}}\frac{\eta_{ik}}{l_{si}} = \rho_{\mathrm{si}}\,\mathrm{d}_{\mathrm{ik}}\,\gamma_{\mathrm{ik}} \tag{5}$$

where l_{si} is the bar length between two cracks.

The stiffening contribution to the steel bar provided by the concrete between two cracks produces a not uniform strain distribution along the reinforcing bar. The

equations governing the problem are the equilibrium relationships for section, for steel bar and for concrete (Figs. 3a,b,c) and the compatibility equation:

$$\frac{\mathrm{ds}}{\mathrm{dx}} = \varepsilon_s - \varepsilon_c \tag{6}$$

where s = u_s-u_c is the slip and u_s and u_c are the steel and concrete displacement along the bar respectively. Combining the previous relations, the solving differential equation is obtained:

$$\frac{\mathrm{d}^2\mathrm{s}}{\mathrm{dx}^2} = \frac{4}{\phi\,\overline{\mathrm{E}}_\mathrm{s}}\left(1+\frac{\overline{\mathrm{E}}_\mathrm{s}}{\overline{\mathrm{E}}_\mathrm{c}}\rho_\mathrm{si}\right)\tau_\mathrm{b}(\mathrm{s}). \tag{7}$$

The bond-slip law of the CEB Model Code 90 [9] is adopted (Fig. 3d). The problem is numerically solved (Fig. 3e) using the FDM (finite difference method) with the boundary conditions $s(0) = 0$ and $s(l_s/2) = \delta/2$. After the evaluation of s, the concrete stresses can be evaluated through the concrete equilibrium equation (Fig. 3c), starting from the known value of the concrete stress in the crack. The concrete strain is then calculated on the basis of the tensile field of the concrete constitutive law and the steel strain along the bar is obtained from Eq. 6 by imposing the symmetry in $x = 0$ and $x = l_s/2$. Finally, this value is corrected in order to assure the equivalence between the mean steel strain obtained from the tension stiffening formulation and the global mean steel strain in the bar direction. The tension stiffening coefficient is evaluated as $\mathrm{g_{ik}} = \varepsilon_{sicrk}/(\delta_{ik}/l_{si})$, where ε_{sicrk} is the steel strain at the crack.

The steel stiffness matrix for the i$^{\mathrm{th}}$ bar crossing the k^{th} crack can be written in the local x_i- y_i coordinate system, where $\overline{E}_{sicrk}$ is the steel secant elastic modulus at the crack corresponding to ε_{sicrk} and ρ_{ik} is steel ratio, as:

$$\left[\mathrm{D}^{\mathrm{x_i y_i}}_{\mathrm{si,crk}}\right] = \rho_{\mathrm{ik}}\begin{bmatrix}\mathrm{g_{ik}}\overline{\mathrm{E}}_{\mathrm{sicrk}} & 0\\ 0 & \mathrm{d_{ik}}\end{bmatrix} \tag{8}$$

Concrete Modeling

Uncracked concrete and concrete between cracks (in this case the mechanical parameters are properly degraded by introducing a damage coefficient) are modeled as an incrementally linear material, orthotropic with respect to the principal strain directions 1-2-3, and associated to a strength domain based on a failure surface closed by a cap surface [1, 10], capturing the concrete failure near the hydrostatic axis (Fig.2e), through the following material stiffness matrix:

$$\left[D_c^{123}\right] = \begin{bmatrix}\left[D_{c,direct}^{123}\right] & [0]\\ [0] & \left[D_{c,shear}^{123}\right]\end{bmatrix} \tag{9}$$

$$\left[D_{c,direct}^{123}\right]=\frac{1}{\Phi}\begin{bmatrix} E_{c1}\left(1-\mu_{23}^2\right) & \sqrt{E_{c1}E_{c2}}\left(\mu_{13}\mu_{23}+\mu_{12}\right) & \sqrt{E_{c1}E_{c3}}\left(\mu_{12}\mu_{23}+\mu_{13}\right) \\ & E_{c2}\left(1-\mu_{13}^2\right) & \sqrt{E_{c2}E_{c3}}\left(\mu_{12}\mu_{13}+\mu_{23}\right) \\ \textit{symm.} & & E_{c3}\left(1-\mu_{12}^2\right) \end{bmatrix}; \quad (10\text{-}11)$$

$$\left[D_{c,shear}^{123}\right]=\begin{bmatrix} G_{c12} & 0 & 0 \\ & G_{c13} & 0 \\ \textit{symm.} & & G_{c23} \end{bmatrix}; \quad \mathrm{G_{cij}}=\frac{1}{4\Phi}\left[E_{ci}+E_{cj}-2\mu_{ij}\sqrt{E_{ci}E_{cj}}-\left(\sqrt{E_{ci}}\mu_{jk}+\sqrt{E_{cj}}\mu_{ik}\right)^2\right]$$

$$\Phi=1-\mu_{12}^2-\mu_{13}^2-\mu_{23}^2-2\mu_{12}\mu_{13}\mu_{23} \;\; ; \;\; \mu_{ij}^2=\nu_i\nu_j \;\; ;$$

being E_{ci} and ν_i the secant elastic modulus and the Poisson coefficient relative to the i^{th} direction, respectively.

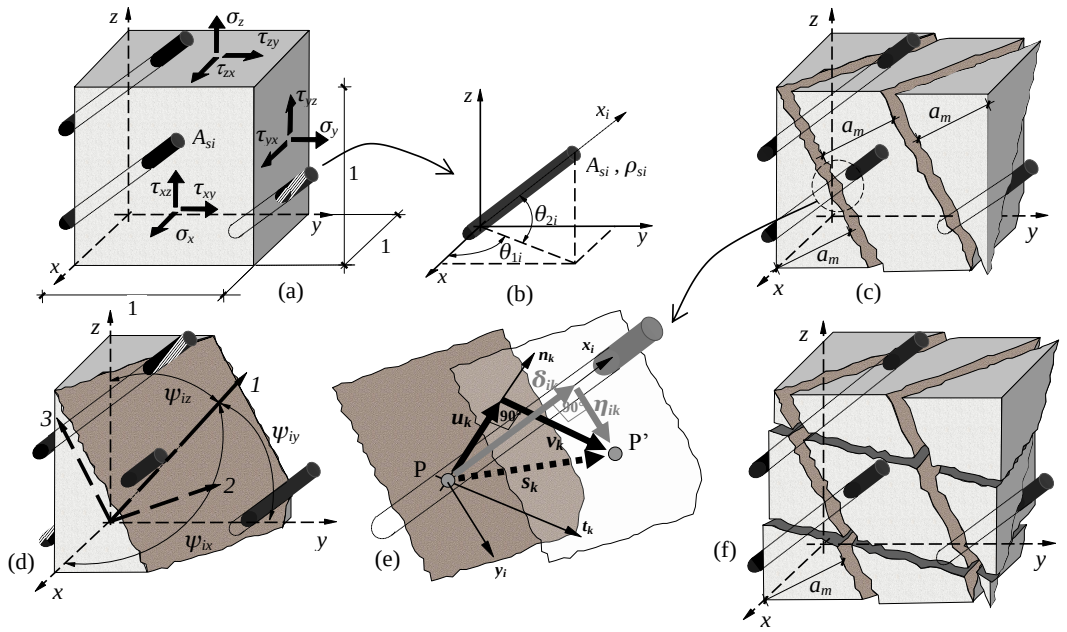

Figure 4. (a) Solid unitary RC element and (b) local steel coordinate system; (c) singly cracked RC element, (d) first cracking condition, (e) crack local coordinate system and displacement definition, (f) doubly cracked RC element.

STIFFNESS MATRIX FOR THE 3D REINFORCED CRACKED ELEMENT

The theoretical formulation refers to a unitary solid element reinforced with steel bars arranged in layers (Fig.4a,b), characterized by their x_i-axis (defined through the angles θ_{1i} and θ_{2i}), having cross-sectional area A_{si}, diameter ϕ_i and geometric steel ratio ρ_{si}. When the principal tensile strain exceeds the tensile strain limit, cracks form perpendicularly to the *1*-axis, which represents the current direction of the maximum tensile strain (Fig.4c,d), being 1-2-3 axes the current principal strain directions. This direction, named n_1, characterizes the orientation of primary cracks, while a_{m1} is the

crack spacing. In the crack plane, the t_1 axis represents the direction of the current slip between crack surfaces (Fig. 4e).

After cracking, the total strain can be divided in two contributions:

$$\{\varepsilon\} = \{\varepsilon_c\} + \{\varepsilon_{cr1}\} \tag{12}$$

where $\{\varepsilon_c\}$ is the reinforced concrete strain between two cracks and $\{\varepsilon_{cr1}\}$ is the resultant primary crack strain. The latter is the transformation into the global coordinate system x-y-z of the crack strain defined in the local coordinate system n_1-t_1 as:

$$\left\{\varepsilon_{cr1}^{n_1 t_1}\right\} = \left\{\frac{u_1}{a_{m1}} \quad \frac{v_1}{a_{m1}}\right\}^T = \left\{\varepsilon_1 \quad \gamma_1\right\}^T \tag{13}$$

being u_1 the crack opening and v_1 the crack slip (Fig. 4e).

The equilibrium in the crack in the *x-y-z* coordinate system can be written as:

$$\{\sigma\} = \{\sigma_{cr1}\} = \{\sigma_{c,cr1}\} + \{\sigma_{s,cr1}\} = \left(\left[D_{c,cr1}\right] + \left[D_{s,cr1}\right]\right)\{\varepsilon_{cr1}\} = \left[D_{cr1}\right]\{\varepsilon_{cr1}\} \tag{14}$$

where $\{\sigma_{cr1}\}$ is the stress in the crack, $\{\sigma_{c,cr1}\}$ and $\{\sigma_{s,cr1}\}$ are the stresses in the crack due to concrete (aggregate bridging and interlock) and to steel (tension stiffening and dowel action) contributions respectively, $[D_{cr1}]$ is the crack stiffness matrix, $[D_{c,cr1}]$ and $[D_{s,cr1}]$ are the stiffness matrices due to concrete and steel contributions in the crack.

The equilibrium of the RC between two cracks can be written as:

$$\{\sigma\} = \{\sigma_c\} + \{\sigma_s\} = \left[D_c\right]\{\varepsilon_c\} + \left[D_s\right]\{\varepsilon_s\} \cong \left[D_c\right]\{\varepsilon_c\} + \left[D_s\right]\{\varepsilon\} \tag{15}$$

where $[D_c]$ and $[D_s]$ are the stiffness matrices of concrete (whose terms are adequately softened by a degradation coefficient, taking into account the damage due to cracking) and steel between the cracks, respectively. The assumption $\{\varepsilon_s\}=\{\varepsilon\}$ is allowed since the average strain of steel between two adjacent cracks, $\{\varepsilon_s\}$, assumes values that are little lower with respect to the average strain $\{\varepsilon\}$ of the element. From Eqs. 14 and 15, the crack strain and the concrete strain are obtained:

$$\begin{aligned} \{\varepsilon_{cr1}\} &= \left[D_{cr1}\right]^{-1}\{\sigma\} \\ \{\varepsilon_c\} &= \left[D_c\right]^{-1}\left(\{\sigma\} - \left[D_s\right]\{\varepsilon\}\right) \end{aligned} \tag{16}$$

which, substituted into the compatibility Eq. 12, yields:

$$\{\sigma\} = \left(\left[D_c\right]^{-1} + \left[D_{cr1}\right]^{-1}\right)^{-1}\left(\left[I\right] + \left[D_c\right]^{-1}\left[D_s\right]\right)\{\varepsilon\} \tag{17}$$

where $[D] = \left(\left[D_c\right]^{-1} + \left[D_{cr1}\right]^{-1}\right)^{-1}\left(\left[I\right] + \left[D_c\right]^{-1}\left[D_s\right]\right)$ is the global RC stiffness matrix and $[I]$ is the identity matrix.

When in the concrete between two adjacent cracks the maximum principal tensile strain, along the *1*-axis assumed as current direction, exceeds the tensile strain limit,

secondary cracks arise (Fig. 4f), perpendicularly to the *1*-axis. This direction (called n_2) characterizes the orientation of secondary cracks and will be kept fixed. Following this approach, the formulation can be generalized to the case of N_{cr} cracks, obtaining:

$$[D]=\left([D_c]^{-1}+\sum_{k=1}^{N_{cr}}[D_{crk}]^{-1}\right)^{-1}\left([I]+[D_c]^{-1}[D_s]\right) \tag{18}$$

where $[D_{crk}]$ is the stiffness matrix of the k^{th} crack.

NUMERICAL IMPLEMENTATION AND MODEL VALIDATION

The 3D-PARC stiffness matrix has been implemented into the FE code ABAQUS through an external subroutine called UMAT (User MATerial). The variables passed in are the material properties and the current stress and strain fields in the structure.

The reliability and the capability of the proposed 3D-PARC model has been verified through the analysis of the global and local behaviour of reinforced concrete elements showing a marked 3D response. To this aim, an hollow square section beam subjected to pure torsion, named T1 [5], has been analyzed through the proposed procedure.

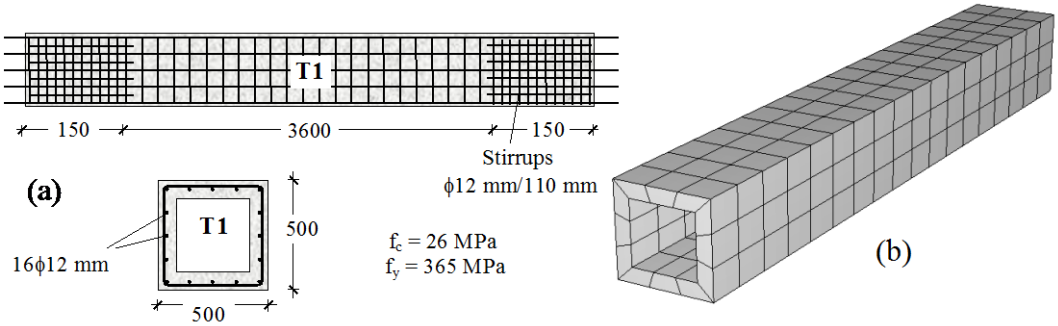

Figure 5. (a) Geometric characteristics and reinforcement arrangement, (b) FE mesh.

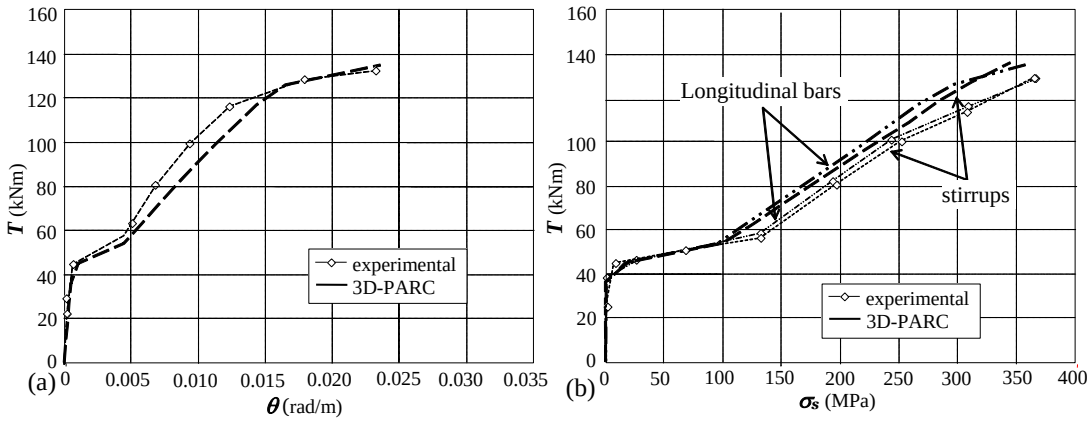

Figure 6. Comparisons between numerical and experimental results: applied torque versus (a) twist; (b) stress in longitudinal bars and in stirrups.

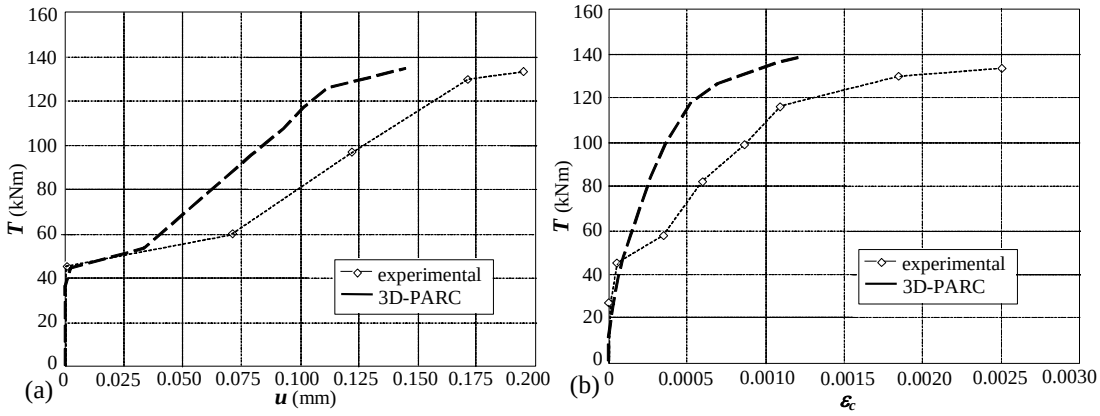

Figure 7. Comparisons between numerical and experimental results: (a) crack opening; (b) concrete compressive strain.

Careful and detailed comparisons between the well-documented experimental results and the numerical ones have been carried out. 20-node quadratic solid elements with reduced integration, called C3D20R, have been used and the adopted FE mesh, consisting of 216 elements and 1572 nodes, is shown in Fig. 5b. Some comparisons between experimental observations and numerical predictions are reported in Figs. 6, 7.

CONCLUSIONS

The comparisons reported in Figs. 6, 7 prove that the proposed procedure is able to accurately describe the fundamental aspects governing the mechanical behavior of the examined structure. In fact, numerical results, as well as experimental observations (Figs.6a,b, 7a,b), show that the beam T1 is characterized by the almost simultaneous yielding of the longitudinal and transversal steel. After the crack formation, the load is equally transferred to the longitudinal and transversal steel, so determining a sudden increment of twist, while concrete struts and cracks show a 45 deg orientation with respect to the beam axis, without subsequent reorientation as loading increases.

References

1. Mordini, A. (2006) Doctorate dissertation, University of Parma, Italy.
2. Cerioni, R., Iori, I., Michelini, E., Bernardi, P. (2006) In: *Proc. Int. CP Conf., on CD.*
3. Cerioni, R., Iori, I., Michelini, E., Bernardi, P. (2008) *Eng. Fract. Mech.* **75**, 615-628
4. Elwi, A.A., Murray, D.W. (1979) *J. Engng. Mech. Division* **105**, EM4, 623-641.
5. Lampert, P., Thürlimann, B. (1968), Bericht Nr. 6506-2, Zürich.
6. Li, V.C., Stang, H., Krenchel, H. (1993), *Mater. Struct.* **26**, 486-494.
7. Gambarova, P.G. (1983) In: *Proc. Giornate AICAP*, 141-156.
8. Walraven, J.C., Reinhardt, H.W. (1981) In: *Heron, Concrete Mechanics*, part A, **26.**
9. CEB-FIP Model Code 90 (1993), **213/214**.
10. Menetrey, P., Willam, K.J, (1995) ACI Struct. J. **92** (3), 311-317.